Green Chemistry

PAPER

Sweet graphene: exfoliation of graphite and preparation of glucose-graphene cocrystals through mechanochemical treatments†

Cite this: DOI: 10.1039/c8gc01162a

Viviana Jehová González,‡[a] Antonio M. Rodríguez,‡[a,b] Verónica León,[a] Javier Frontiñan-Rubio,[a,c] José Luis G. Fierro,[d] Mario Durán-Prado,[c] Ana B. Muñoz-García,[e] Michele Pavone[b] and Ester Vázquez *[a,f]

Received 12th April 2018,
Accepted 2nd July 2018

DOI: 10.1039/c8gc01162a

rsc.li/greenchem

Mechanochemical treatment with carbohydrates leads to the successful exfoliation of graphite and this can be considered as a green approach to the preparation of graphene. Glucose, fructose and saccharose were used and the former showed the best exfoliation behaviour to generate graphene materials with a relatively low number of defects, as evidenced by Raman spectroscopy. The addition of small amounts of water to the ball milling treatment led to the formation of glucose-graphene co-crystals, which exhibited superior properties in terms of colloidal stability and minimization of cell toxicity.

Introduction

Green Chemistry protocols are being gradually transferred to the design of nanomaterials, with the preparation of gold and silver nanoparticles being successful examples of this trend.[1–3] However, every nanotechnology follows its own journey and carbon nanomaterials still provide challenging opportunities for the development of green approaches, which could minimize toxicity and enhance the functionality of the final products.

Of the different carbon nanomaterials, graphene has emerged as a promising entity in numerous applications, including biological systems, and continuous efforts are committed to translating the novel material properties into real products and innovative technologies. However, despite the fact that there are different approaches to produce graphene materials and some of these products are starting to be produced at industrial scale,[4] many of these synthetic processes require the use of toxic solvents such as DMF and NMP[5] and/or harsh conditions and corrosive acids,[6] which also produce hazardous wastes. Several studies have already been published on the preparation of graphene materials by sustainable methodologies such as electrochemical exfoliation in water,[7] sonication in water/alcohol,[8] or sonication with natural compounds,[9] liquid exfoliation in water,[10,11] and supercritical fluids.[12–14] In other studies the exfoliation of graphite in water has been performed using pyrene derivatives,[15–17] anionic surfactants,[18] polymers[19] or proteins.[20,21] However, these methodologies normally suffer from low yields (around 10% in weight), low concentrations of final material and/or low stability of the aqueous dispersions.[22] Therefore, there is still a need to design protocols for the preparation of graphene materials in a sustainable way.

Increased funding has been committed to assess the environmental and health impact of graphene materials as well as its application in biomedicine.[23] While significant advances have been made, the main challenge concerns the poor stability of graphene materials in aqueous systems. This drawback is usually overcome with the use of surfactants or co-solvents,[24,25] which are often contaminants. An alternative option is to increase the surface oxygenation of the final material by preparing graphene derivatives such as graphene oxide, a material with completely different properties.[26,27]

The demanding situation outlined above offers extensive research opportunities. How can we design a water-soluble graphene material that is suitable for use in biomedical studies without changing the chemical characteristics of graphene? Can this design be optimized for green chemistry principles

[a]Instituto Regional de Investigación Científica Aplicada (IRICA), UCLM, 13071 Ciudad Real, Spain
[b]Dipartimento di Scienze Chimiche, Università degli Studi di Napoli Federico II, Via Cinthia, Naples, Italy
[c]Cell Biology area, Faculty of Medicine, University of Castilla-La Mancha, 13071 Ciudad Real, Spain
[d]Instituto de Catálisis y Petroleoquímica, CSIC, Cantoblanco, 28049 Madrid, Spain
[e]Department of Physics "Ettore Pancini", Università degli Studi di Napoli Federico II, Via Cinthia, Naples, Italy
[f]Facultad de Ciencias y Tecnologías Químicas, UCLM, Avda. Camilo José Cela S/N, 13071 Ciudad Real, Spain

†Electronic supplementary information (ESI) available. See DOI: 10.1039/c8gc01162a

‡These authors contributed equally to this work.

such as energy minimization, waste reduction and safe solvents and reaction media?

Pharmaceutical companies have long dealt with solubility problems. Most of the new active pharmaceutical ingredients (API) display poor aqueous solubility, mainly due to the increase in molecular size. This issue has commonly been solved by the preparation of salts, but what can be done with non-ionizable drugs? One solution is provided by the formation of cocrystals.[28–30] Pharmaceutical cocrystals are generally formed by an API and compounds known as GRAS (Generally Regarded As Safe). The modular nature of cocrystals has opened up a vast area of opportunity for effective therapies and has transformed biologically active compounds into viable products by providing remediations for a variety of problems, including poor hydration stability,[31] compressibility,[32] poor thermal properties,[33] low solubility and insufficient dissolution rates.[34]

Mechanochemical methods are recognized as the most effective ways to generate cocrystals.[35] Different groups have demonstrated that cocrystals can be formed in neat grinding processes, *i.e.*, by simply grinding the solid reactants together. The grinding can be conducted either manually, using a mortar and pestle, or in a ball milling process. However, the best results are frequently obtained by Liquid Assisted Grinding (LAG),[36,37] in which small amounts, even molar equivalents, of solvents can dramatically accelerate cocrystal formation.

Mechanochemistry has also gained increasing importance in the preparation and functionalization of carbon nanostructures.[38–40] Mechanochemical protocols have many advantages over their liquid-phase counterparts, including processes with shorter reaction times, higher product yields and the elimination of (harmful) organic solvents, which make the approach more sustainable. In this sense, mechanochemistry has been successfully applied for the low-cost mass production of graphene.[41] Ball-milling of graphite has been performed with dry ice,[42] cellulose[43] and other natural compounds.[44] However, these methodologies still have limitations when producing aqueous graphene dispersions with reasonable concentrations in water and culture media[45] and they are not suitable for biological applications.

The aim of the work described here was to develop an environmentally friendly, economical and simple approach for the synthesis of water-soluble graphene materials that would be useful for biological purposes. We also considered green chemistry objectives such as energy efficiency, process safety and waste reduction. With this goal in mind, we relied on abundant, renewable and non-toxic carbon resources, *e.g.*, carbohydrates, as exfoliating agents for graphite through a mechanochemical process under solvent free conditions. Theoretical studies were performed in order to tune the exfoliation process. The final graphene material was thoroughly characterised and we also evaluated the formation of possible glucose-graphene cocrystals. The stability of the final materials in aqueous systems was analysed and it was confirmed that graphene-glucose cocrystal powders give higher performance in terms of stability of aqueous dispersions. Moreover, preliminary toxicological tests were carried out to investigate the safety of the designed materials.

Results and discussion

Theoretical study of exfoliation of graphite with carbohydrates

As a first step, we aimed to understand, from a theoretical point of view, if carbohydrates could act as exfoliation agents for graphite. The carbohydrates investigated were sucrose, glucose and fructose.

Sucrose is a disaccharide combination of the monosaccharides glucose and fructose. The structural data for glucose and fructose were extracted from the same XRD structure of sucrose.[46,47] Based on our experience in the theoretical study of the exfoliation of graphite with melamine,[48] density functional theory (DFT-D) was used to investigate the interaction of sucrose, glucose and fructose with graphene. The case of glucose is represented in Fig. 1 (data for sucrose and fructose are collected in Fig. S1 & S2,† respectively). The total adsorption energies ($E_{\text{ads-SWE}}$) are favourable for all three carbohydrates (see Table S1†) and they have been further decomposed into three main contributions:

$$E_{\text{ads-SWE}} = E_{\text{G-SWE}} + E_{\text{G-dist}} + E_{\text{SWE}} = (E_{\text{G-SWE}} - E_{\text{G}''} - E_{\text{SWEnet}}) + (E_{\text{G}''} - n{\cdot}E_{\text{G}}) + (E_{\text{SWEnet}} - m{\cdot}E_{\text{SWE}}) \quad (1)$$

where $E_{\text{G-SWE}}$ is the total energy of the system, $E_{\text{G}''}$ and E_{G} the energies of the supercell and the unitary cell of graphene, respectively; and E_{SWE} is the energy of an isolated carbohydrate molecule (n and m are the number of graphene unit cells and molecules, respectively). From this analysis one can determine the direct interaction energy between the total carbohydrate supramolecular network and graphene ($E_{\text{G-SWE}}$), the distortion

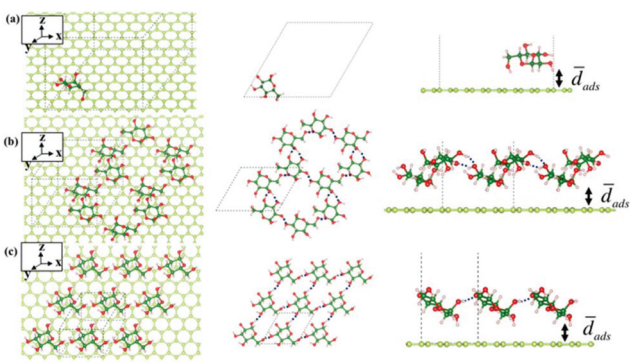

Fig. 1 (a) Isolated molecule of glucose on graphene (right); (b) loose supramolecular network of glucose on graphene; (c) compact supramolecular network of glucose on graphene. View corresponds to perspective (right), topside view (from *z* axis, on centre), lateral view (from *x* axis, left). Colour code: carbon graphene (light green), carbon carbohydrate (dark green), nitrogen (light blue), oxygen (red) and hydrogen (light pink). For equilibrium distances (d_{ads}) see Table S1.†

energy of graphene from its unperturbed equilibrium structure ($E_{G\text{-dist}}$) and the cohesive energy of the carbohydrate supramolecular network (E_{SWEnet}). The decomposition of the adsorption energies is collected in Fig. 2 and Table S1.†

In previous studies we have shown the ability of melamine to behave as an exfoliating agent for graphite.[49,50] In comparison to our previous theoretical study, we observed similar adsorption energies for the isolated molecules ($E_{ads} \sim -0.5$ eV).[48] The interaction between the carbohydrates and graphene is produced by the hydroxyl groups (–OH), which behave in a similar way to the amino groups in melamine.[49,51]

The supramolecular network was selected to maximise the covered area of graphene and to exploit the maximum number of intermolecular interactions. As coverage increased, *i.e.*, from loose (**L**) to compact (**C**), similar behaviour of the adsorption energies was observed as in the melamine studies. Both $E_{G\text{-SWE}}$ and E_{SWEnet} became more negative and this contributed to the overall adsorption energies. In this case, glucose and fructose gave the most marked gain in E_{SWEnet} in the loose network (**L**), which indicates a better disposition to form supramolecular networks: when the carbohydrates interact with each other, the –OH groups are partially involved in the carbohydrate-graphene interaction.

However, the abundance of –OH groups in these molecules makes the effects less significant than with melamine. A similar elongation of the average distance between all carbohydrates and the graphene layer was also observed (Table S1†). Moreover, the carbohydrate adsorption on increasing coverage did not affect the planar structure of graphene. The distortion energies $E_{G\text{-dist}}$ listed in Fig. 2 are very similar in all cases and are close to zero in the supramolecular networks. Consequently, the graphene electronic structure retains its main features, as shown by the calculated Projected Density of States (PDOS) in Fig. S3 in the ESI.†

The variation in E_{SWEnet} represents the energy contribution from the intermolecular H-bond network. The formation of the supramolecular networks is driven by the strength of the H-bonding interactions (around −0.19/−0.37 eV) (Table 1). The E_{SWEnet} energy variation (around 0.2/0.3 eV) depends on the different intermolecular interactions at different coverage levels and it is a result of the degrees of freedom of the multiple –OH groups.

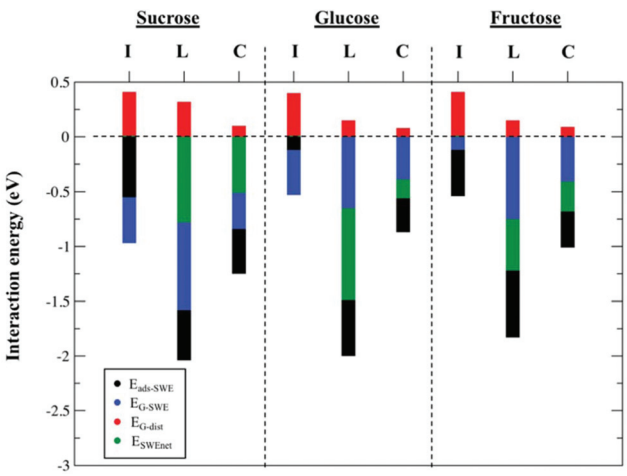

Fig. 2 Decomposition of adsorption energies (eV) on the isolated (**I**), loose (**L**) and compact (**C**) supramolecular network of carbohydrates on graphene.

Table 1 Analysis of the carbohydrate supramolecular networks: interaction energy (E_{SWEnet}), number of interacting units (No. inter) and normalized interaction energies

		E_{SWEnet} (eV)	No. inter.	$E_{ads\text{-}SWE}$/No. inter (eV)
L Network	Sucrose	−0.78	4	−0.19
	Glucose	−1.49	4	−0.37
	Fructose	−1.22	5	−0.24
C Network	Sucrose	−0.51	2	−0.26
	Glucose	−0.56	2	−0.28
	Fructose	−0.68	2	−0.34

From the theoretical perspective, glucose can act as a better exfoliating agent given that the formation of the supramolecular network leads to a higher energy gain than for the other molecules. Moreover, these interactions are in the same energy range as those predicted for other exfoliating agents and H_2O interactions,[48] which is considered to be the driving force for the stabilization of supramolecular systems such as melamine-graphene in aqueous dispersions.

Mechanochemical production of few-layer graphene (FLG) using glucose as exfoliating agent

In an effort to confirm the theoretical results, we compared the exfoliation of graphite using melamine (sample 1), glucose (sample 2), sucrose (sample 3) and fructose (sample 4) as exfoliating agents in the mechanochemical treatment of graphite.

In a first approach, and as a comparison, the experimental conditions reported previously by us for the melamine exfoliation of graphite[45,49,52] were used for the preparation of FLG by ball-milling treatment. In a typical experiment, 7.5 mg of graphite and 0.16 mmol of the carbohydrate or melamine were ball-milled at 100 rpm for 30 min in a stainless-steel grinding bowl with ten stainless steel balls (1 cm diameter) in an air atmosphere. After the treatment, the resulting solid mixtures were dispersed in 20 mL of water to give a black dispersion in each case. The exfoliating agent was removed and recovered by dialysis (see ESI†).[45,49,52] The final dispersions (Fig. 3) were stable at room temperature for several weeks. A comparison between the dispersions obtained using the different exfoliating agents can be made from the results in Table 2. The highest graphene concentration was obtained on using melamine, closely followed by glucose (Table 2).

The experimental results are in good agreement with the theoretical insight, and glucose was proposed as a good substitute for melamine in the exfoliation of graphite while avoiding the use of a toxic starting material (melamine) in the preparation of graphene.

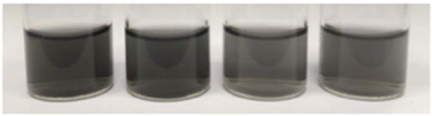

Fig. 3 Photographs of graphene solutions in water. The exfoliating agents used were: melamine (sample 1), glucose (sample 2), sucrose (sample 3), fructose (sample 4).

Table 2 Comparison of the effectiveness of exfoliating agents as stabilizers for graphene in water

Sample	Exfoliating agent	Graphene concentration (mg mL^{-1})	Concentration of exfoliating agent (mg mL^{-1})
1	Melamine[a]	0.09	0.0009
2	Glucose[b]	0.04	0.26
3	Sucrose[c]	0.022	0.25
4	Fructose[b]	0.018	0.33

[a] Melamine was detected using UV protocols published by our group.[53] [b] Glucose and fructose concentrations were calculated using a UV-test from Boehringer Mannheim. [c] Sucrose concentration was measured *via* refractometer measures.

Further studies were carried out to optimise the exfoliation of graphite using glucose. Experiments were performed using similar mechanochemical treatments under solvent-free conditions, which were denoted as neat grinding conditions. Huang *et al.* described the use of polysaccharides and other thermoplastic polymers as exfoliation agents for graphite in ball milling treatments.[43] They also attempted the use of glucose as an exfoliating agent without success and only observed glue-like materials. In the work reported here the milling conditions were modified in order to avoid glucose melting.

We first optimized the treatment time with a fixed ratio of graphite/glucose (75 mg graphite and 4.5 g of glucose) in a 250 mL stainless-steel grinding bowl with 15 stainless steel balls (2 cm diameter each) at a 250 rpm. After the treatment, the resulting solid was suspended in 100 mL of water, sonicated for 1 min and centrifuged at 1500 rpm for 15 min. The samples were subsequently dialysed to remove glucose and the final aqueous graphene dispersions were lyophilised at −80 °C at a pressure of 0.005 bar (see ESI† for Experimental details). Glucose was recovered from the permeate (up to 85–90%). Characterization of the recovered material by NMR spectroscopy (Fig. S4†) confirmed that glucose had not been modified during the milling treatment, which allowed this material to be reused for further exfoliation. This finding is consistent with the established principles of Green Chemistry for reducing waste and reusing materials.

The treatment outlined above afforded dry powdered graphene materials and these were characterised by Raman spectroscopy to determine the conditions that provided the best final product. The results of the Raman study provided the

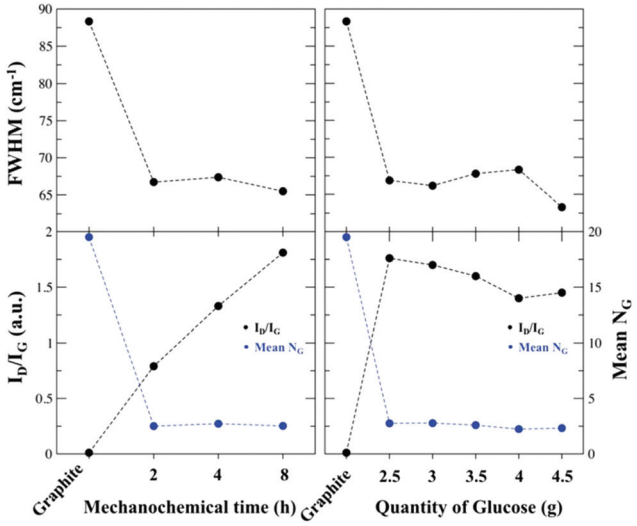

Fig. 4 2D band FWHM values and I_D/I_G values in Raman spectra for FLG prepared with different glucose ratios and ball milling times (in hours).

relation between the intensities of D (I_D), G (I_G) and 2D (I_{2D}) bands present in carbon nanomaterials (see Fig. 4).[54,55] The full width at half maximum (FWHM) of the 2D band provides information on the average thickness of the graphene sheets[56,57] and narrow 2D bands have been reported for a low number of layers. Moreover, the number of layers (N_G) in the final graphene material was calculated from the equation described by Coleman *et al.*,[58] using the information obtained from the 2D band positions, and the intensity ratio between the D and G bands (I_D/I_G) was used to quantify the density of defects in the graphene (Fig. 4).[59,60]

A direct correlation was observed between long mechanochemical treatments and a high number of defects. The graphene presented the highest I_D/I_G (around 1.8) after a grinding time of 8 h. Regarding FWHM and N_G, very few differences were observed between 2 and 8 h of mechanochemical treatment. However, the final yield in the graphene production was very different, with graphene yields of 20 and 47%, respectively, obtained for grinding times of 2 and 4 h, as calculated from the starting mass of graphite. A treatment time of 8 h gave a very low quantity of graphene material (<10% in mass).

Finally, the variation of the ratio between graphite (75 mg) and glucose (from 2.5 to 4.5 g) was studied for a mechanochemical treatment time of 4 h. On using less than 2.5 g of glucose a very low yield of graphite exfoliation was observed. In general, similar data were observed for I_D/I_G and N_G, and the main differences were observed in the FWHM, with a narrow 2D band observed for the treatment with 4.5 g of glucose.

In view of these results, we further characterised the graphene material obtained with the best milling conditions, denoted as **Neat 2h** and **Neat 4h** (75 mg of graphite and 4.5 g of glucose and 2 and 4 h of ball milling, respectively). A representative Raman spectrum of **Neat 2h** is shown in Fig. 5. The I_D/I_G values were around 0.7 and a low N_G (2–3 layers) was

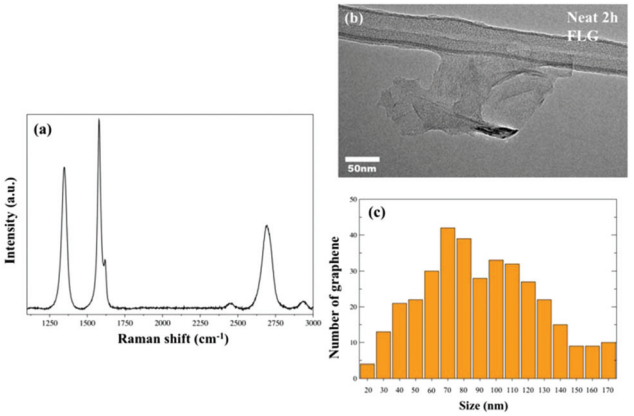

Fig. 5 Characterization of graphene from Neat 2 h conditions (a) Raman spectra, (b) TEM Image and (c) size distribution.

observed (Fig. 4). The size distribution of **Neat 2h** graphene is very homogeneous, with an average size of 120 nm.

Neat 4h exfoliation conditions (Fig. 6) gave two different populations of graphene materials, namely **FLG1** (FLG of <100 nm, average of 50 nm) and **FLG2** (FLG of 100–300 nm). The possibility of obtaining graphene materials of different sizes for use in biological studies is considered a challenging task. Some authors have already shown different cell responses on using graphene oxide of different dimensions.

The high yield obtained in Neat 4 conditions allowed the separation of the different populations by simply allowing the water dispersion to stand for 5 days. **FLG1** was obtained in the supernatant of the solution, while **FLG2** was present in the lower sections of the solution. The TEM images in Fig. 6 are representative of the graphene samples. A statistical analysis of **FLG1** samples (<100 nm) showed that the major components are graphene flakes of around 40 nm and **FLG2** graphene with a different size distribution, between 100–300 nm (centred on 180 nm), which has a lower aggregation effect. Additional HRTEM and SAED data for the samples are included in the ESI (Fig. S5†).

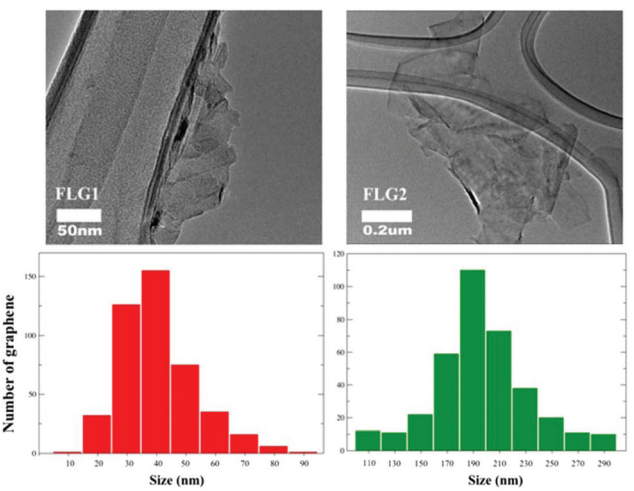

Fig. 6 TEM image of FLG1, FLG2 for Neat 4 h and the relative size distributions of graphene sheets.

Both **FLG1** and **FLG2** have similar Raman spectra (Fig. 7). The I_{2D}/I_G ratio, with values of less than 1, confirms the presence of few-layers graphene (Fig. 7(a)).[61] The I_D/I_G ranges from 1.4 to 1.2 (Fig. 7(b)) and **FLG1** has a higher value, which correlates with smaller flakes.

If we compare the BET value obtained for graphene prepared using glucose as exfoliating agent (134 m^2 g^{-1}, data in the ESI of this manuscript, Fig. S6†) with the one of graphene prepared using melamine (10 m^2 g^{-1}),[62] the value is much higher for the material described in the present manuscript. However, the theoretical surface area of pristine graphene is 2630 m^2 g^{-1}.[63] Some authors have already pointed out that BET surface areas of dry powders are affected by the agglomeration of the material in the powder.[64] In this sense, the hypothetical data of pristine graphene could be observed if no overlaps between the sheets exits in the solid powder. The fact that graphene prepared using glucose is smaller and present a higher number of edge defects agrees well with this idea of less agglomeration in the dry powder and correlates with the a lower thermal stability observed by TGA.

Thermogravimetric analysis (TGA) of FLG1 and FLG2 was performed under an inert atmosphere (Fig. S7†). FLG2 is more stable than FLG1 and this corresponds to the lower number of defects observed by Raman spectroscopy. The average weight loss at 600 °C in FLG1 samples is 33% (9% for FLG2). This is due to pyrolysis of the residual oxygen-containing groups at the edges or on the graphene surface.[65] The two principal weight losses between 200 °C and 400 °C involve the evolution/decomposition of oxygen functional groups, firstly the carboxylate groups (RCOO–), which seems to be more significant in

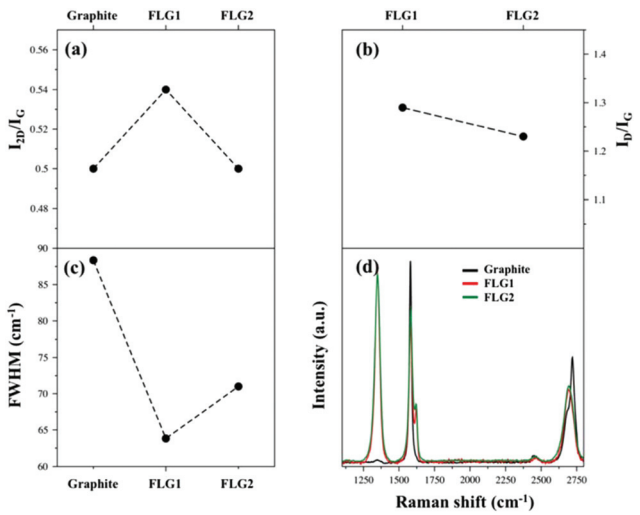

Fig. 7 Raman Spectroscopy data for the synthesis of Neat 4 h; (a) relation between I_D/I_G and I_{2D}/I_G bands; (b) G and D band positions; (c) FWHM of 2d band; and (d) Raman spectra for graphite, and FLG1 and FLG2 from Neat 4 h.

Table 3 Total percentage (%) of C and O groups for **FLG1** and **FLG2**

Sample	%C	%O
FLG1	86.7	13.3
FLG2	92.5	7.5

FLG1, and then the carbonyl (C═O) and the rest of the oxygenated groups.[65] TGA under air of FLG1 and FLG2 are presented in Fig. S7,† where it is evident that FLG2 has a higher thermal stability than FLG1. The lower thermal stability of FLG1 could indicate the presence of a higher number of oxygen groups, which could be related to the size of the layers. In this sense, our TGA results correlate well with the XPS data[67,68] (see below).

XPS was employed to evaluate the type and abundance of oxygen groups in the samples (Fig. S8† and Table 3). The C 1s core-level spectra were fitted with Gaussian–Lorentzian (90G/10L) peaks to give four or three main components with different binding energies: 284.5 eV (sp^2 carbon bonds, non-oxygenated ring C), 286.4 eV (sp^3, C–O–C bond), 287.8 eV (C═O bonds) and 289.3 eV (C(O)O bonds).[66] The relative area of the peak corresponding to the sp^2 bonds is higher for **FLG2** and this is consistent with the Raman spectra. Overall the O-content in **FLG1** is higher than in **FLG2** and the distribution of oxygenated groups is different in each sample (Fig. S8†). In **FLG1** a higher number of carboxylic groups is observed and this is consistent with the TGA curves. A wide scan XPS spectra has been included in the ESI (Fig. S8†).

Finally, the colloidal properties of graphene in water were evaluated by UV-Vis absorption spectroscopy at 660 nm. The absorption values can be correlated with the concentration of the lyophilized graphene powders after re-suspension in deionised water.[45] These re-dispersions of **FLG1**, **FLG2** in water were performed at different initial concentrations (0.2, 0.1 and 0.05 mg mL^{-1} in Fig. 8).

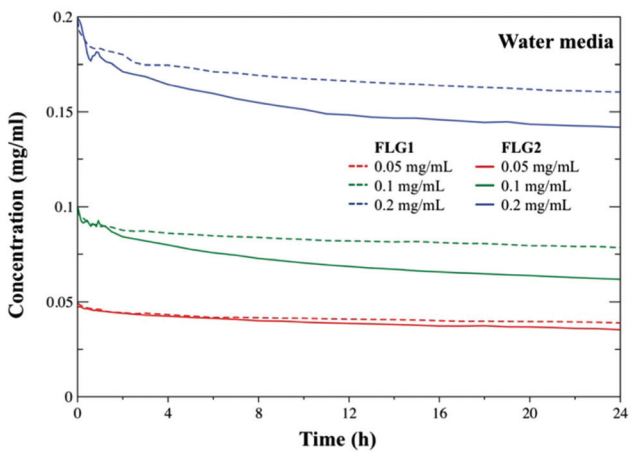

Fig. 8 Stability of FLG in deionised water for FLG1 and FLG2 from Neat 4 h sample for 24 h.

FLG1 showed higher stability, with a sedimentation below 20% after 24 h, while **FLG2** showed a sedimentation range of 30–40% at the same time. In aqueous dispersions, particle motions result in collisions that may give rise to agglomeration and can eventually produce sedimentation. The formation of these aggregates depends on the initial size of the graphene flakes and the surface chemistry, which explains the better colloidal stability of the smaller flakes (**FLG1**). The process is faster in the first few hours and then it becomes stationary.

Several conclusions can be drawn in terms of differences between melamine and glucose as exfoliating agents for the preparation of graphene. Firstly, exfoliation with melamine is easier than with glucose and longer milling times and a higher ratio between glucose and graphite are required. However, the size of the final graphene material can be modified easily upon using glucose to obtain products with higher stability in aqueous media. Moreover, the greatest advantage of this methodology is that it avoids the use of toxic melamine, which makes the present material ideal for biological experiments and applications.

Mechanochemical synthesis of graphene-glucose cocrystals

As described in the previous section, only graphene flakes with very small sizes are able to form colloidal dispersions in water and these are stable for several hours but mainly have very low concentrations. If higher concentrations are required precipitation occurs – mainly during the first 2 h – and this may be a concern in biological studies. As discussed in the introduction, the formation of cocrystals could provide a way to increase the dispersion of the solid samples in aqueous suspensions by simply changing their solid-state condition without modifying their chemical structure.

Glucose has already been used as a GRAS compound in different models, for example to increase the stability of lithium salts as an improvement in the development of new lithium therapeutics.[69] Following this idea, and having proved that glucose can behave as a good exfoliating agent, we investigated the formation of possible glucose-graphene cocrystals.

It has been reported that the formation of cocrystals can be achieved by simple exposure of solid mixtures to water and subsequent lyophilisation.[70] As a consequence, the mechanochemical treatment described in the previous section (**Neat 2h** and **Neat 4h**) was applied and the resulting graphene-glucose solids were suspended in 100 mL of water, sonicated and centrifuged at 1500 rpm for 15 min. Dialysis was not performed in this case and the samples were subsequently lyophilised at −80 °C at a pressure of 0.005 bar. Finally, the solid samples were characterised, without further treatment, by PXRD and Raman spectroscopy (see ESI† for further information).

The PXRD study showed that Neat samples mostly consisted of glucose and graphene. The pattern in Fig. 9 mainly contains glucose peaks for **Neat 2h** (**Neat 4h** in Fig. S9†). The reduction of the characteristic 26.5° graphite peak corresponding to the surface (002) can be associated with highly efficient graphite exfoliation (Fig. S10†), as described in the literature.[71] The intensity of this peak cannot be observed due to the higher

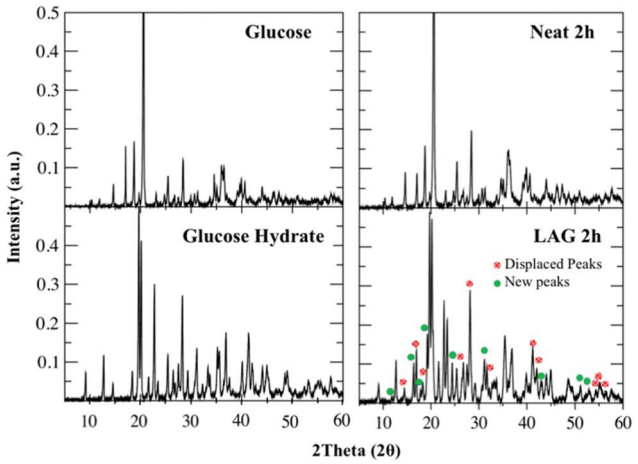

Fig. 9 Powder X-ray diffraction results for glucose, glucose hydrate and neat /LAG conditions for the formation of exfoliated graphene on cocrystals.

presence of the glucose peaks. Other peaks that could be assigned to the formation of a cocrystal structure were not observed for any of these neat conditions.

In view of these results outlined above, it was decided to use Liquid Assisted Grinding (LAG) conditions, which are known to favour the formation of cocrystals. In this second approach the mechanochemical procedure was modified by introducing small quantities of deionized water. The experimental process consisted of the introduction of graphite (75 mg) with 4.5 g of glucose and 2.5 mL of water in a 250 mL stainless steel grinding bowl with 15 stainless steel balls (2 cm diameter each). These samples were ball-milled at 250 rpm for 2 or 4 h. Finally, the solid samples were suspended in 100 mL of water and centrifuged and lyophilised under the same conditions as for the neat samples. The final amount of graphene in these samples was calculated with respect to the 1 mg powder sample in 1 mL of deionized water (Table 4). The graphene percentage was obtained after linear calibration with known quantities of graphene and glucose mixtures at 660 nm and was corroborated by the analysis of glucose calculated in a UV-test from Boehringer Mannheim (see ESI, Fig. S11†).

It can be seen from the results in Table 4 that the amount of graphene is very similar in Neat and LAG samples, although PXRD and Raman spectroscopy revealed different results.

Regarding the PXRD on the LAG sample, a relevant number of new and displaced peaks was observed in comparison to glucose and glucose hydrate, which could indicate the presence of cocrystal structures (Fig. 9 LAG 2h, Fig. S12† LAG 4h).[72] The cocrystal reflections are present in the peaks in the 10–15° and the 22–55° regions, where the biggest modifications are observed and new peaks appear. It seems that the presence of water in the exfoliation process is required in order to produce the cocrystals. These findings are in line with those described by Zaworotko *et al.*, who showed that in a system with an imbalance in the number of acceptor and donor molecules, water molecules could help to stabilise the cocrystal structure.[73] Analysis of the HRTEM images of LAG samples (Fig. S13†) showed that the observed crystal structure had interplanar distances in the range 4.2–4.7 Å, which could correspond to the appearance of the 2theta angle in the range 18.9–21.3°. These angles are similar to those of some of the new peaks observed in the cocrystal.

The Raman spectrum was recorded for each sample and these spectra provide information on the vibrational mode frequencies of the intermolecular and intramolecular bonds but can also give information on the quality of the exfoliated graphene. The results for the neat grinding are consistent with those of the PXRD study: only glucose and graphene bands were observed for both **Neat 2h** and **Neat 4h** (Fig. 10 and Fig. S14†), with the graphene bands being the main component. However, LAG samples showed graphene bands together with new bands that differed from the glucose and glucose hydrate bands, which could result from the supramolecular formation of a cocrystal structure (Fig. 10D). These results are in good agreement with the PXRD results.

The quality of the graphene in the possible cocrystals was further investigated by studying the variation in the intensities of the graphene bands in the Raman spectra (Fig. S15†). The study focused on the ratio of the intensities of the D and G bands (I_D/I_G). The results are collected in Fig. S15† (LAG 4h in Fig. S16†) and they show that the LAG conditions produce a decrease in the number of defects in the structure of graphene in comparison with the neat samples. The FWHM data for the

Table 4 Graphene content (%) in Neat and LAG samples

	Neat 2h	Neat 4h	LAG 2h	LAG 4h
Graphene[a] (%)	2.9	3.2	2.4	2.2

[a] Graphene content determined from a 1 mg sample of cocrystal measured by UV at 660 nm (ESI).

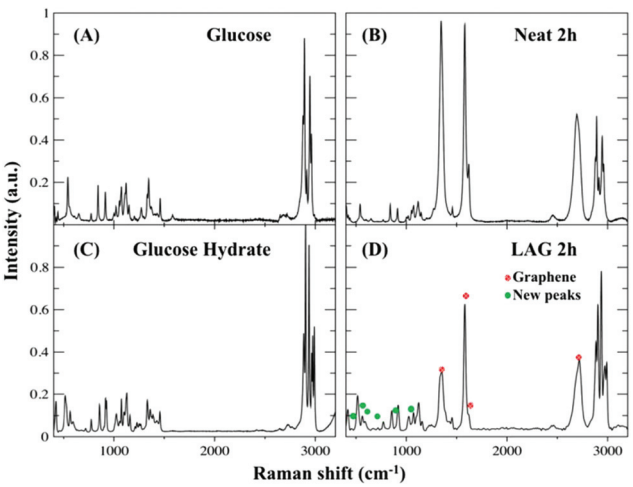

Fig. 10 Raman results for glucose, glucose hydrate and neat/LAG conditions for the of exfoliated graphene on cocrystals.

Table 5 Temperatures from dTGA results for neat grinding and LAG samples from cocrystals samples

Temp. lost (°C)	Glucose	Glucose hydrate	Neat 2h	Neat 4h	LAG 2h	LAG 4h
1st	—	113.5	—	—	95.6	97.6
2nd	231.1	220.3	224.8	223.8	204.4	197.6
3rd	306.4	269.5	291.7	290.8	257.8	250.0

2D peak were also obtained and these show the number of layers in the graphene sample (N_G).[58] The best results were obtained for LAG conditions at 2 h, with an FWHM of 57 cm^{-1} and N_G of 2–3 layers. TGA was carried out to analyse the possible cocrystals (Fig. S17†). Neat samples had similar thermal stability to glucose samples, with two principal weight losses, which take place at around 200 °C and 400 °C. These thermograms present the typical shape for glucose,[74] which supports the idea that neat samples are simply amorphous mixtures of glucose and graphene. The LAG samples, however, showed differences when compared to glucose. These samples display an initial loss (average between 7–10%) at around 97 °C. This could be due to the structural water present in the cocrystal samples. LAG samples had lower thermal stability, as can be observed from the second and third weight losses (Table 5). This behaviour has also been observed for other cocrystals,[75] but this is the first cocrystal sample involving carbon nanostructures and its behaviour is mostly underexplored. Finally, after the weight loss at 600 °C for all neat and LAG samples only around 10–20% of the material remained.[74]

The colloidal stability of graphene was evaluated by UV-Vis absorption spectroscopy at 660 nm to determine the concentration of graphene in FLG (**Neat 4h**) and Cocrystal (**LAG 2h**) samples over time (Fig. 11). These samples were re-dispersed in water and culture media at different initial concentrations (0.2, 0.1 and 0.05 mg mL^{-1}). A higher stability was observed for graphene in the cocrystal sample in comparison with FLG. Partial sedimentation of FLG in water occurred after the first 10 h. The average sedimentation levels of FLG and cocrystal samples in water solutions after 24 h are 48.9% and 19.5%, respectively. It is known that carbon nanostructures are stabilized when dispersed with serum derivatives (such as fetal bovine serum, FBS), the proteins of which are able to cover the nanostructure surfaces and thus improve long-term colloidal stability.[76,77] This behaviour has already been studied in our research group.[45] For this reason, it was decided to analyse the colloidal stability of both FLG and glucose-FLG cocrystals in culture media (supplemented with FBS and an antibiotic), which are the most useful media for biological studies. In these culture media, the stability of both samples were improved but the cocrystal samples had a slightly better profile. The average sedimentation levels for FLG and cocrystals in culture media after 24 h were 31.1% and 22.6%, respectively.

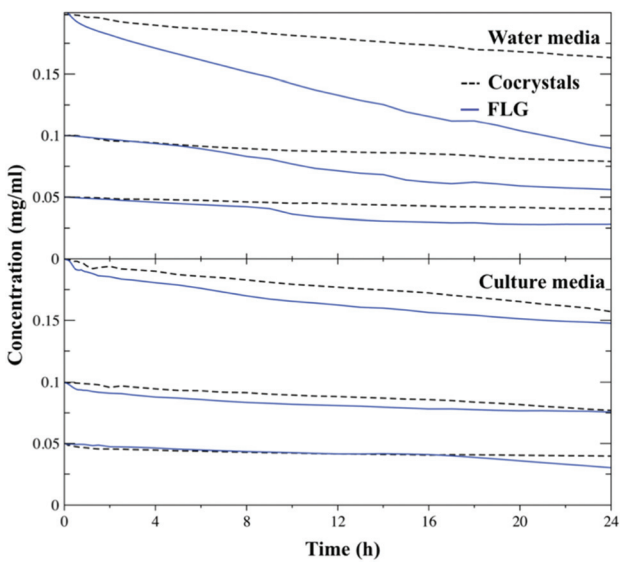

Fig. 11 Stability of FLG in water and culture media for cocrystals and FLG during 24 h.

Toxicity of FLGs on human skin cells

Preliminary studies were carried out to determine whether the formation of glucose-graphene cocrystals affects the ability of FLG to interact with human cells, and specifically with human barriers. For this reason, the effects of FLG prepared by neat and LAG conditions on human skin keratinocytes (HaCaT) were compared, in particular, samples denoted as Neat 2h and LAG 2h in the present work. Human skin keratinocytes (HaCaT) were employed and this is a non-transformed cell line used as standard *in vitro* model to study cutaneous toxicity. It has been previously reported that different GRMs such as GO, FLG, GQDs, *etc.*, could induce cell toxicity and promote apoptosis and necrosis in diverse transformed and non-transformed cell lines including HaCaT.[78–80]

The combination of FLGs with other molecules could determine their ability to interact with human cells and tissues. In fact, some authors have already described the ability of glucose and other monosaccharides to passivate the nanoparticle surface and affect the internalization into the cell. Glucose coating can also affect the protein corona composition, biodistribution and *in vivo* biodegradation.

The results obtained in this study indicate that the two materials produce a dose-dependent reduction of the total number of cells after 24 h treatment with the glucose-FLG cocrystals or FLG, with the effect only being significant at high doses of 100 μg mL^{-1} (Fig. 12, left-hand graph). This decrease in the number of total cells is due to a parallel induction of necrosis (Fig. 12, right-hand graph) and apoptotic-programmed cell death (Fig. 13), with the latter effect being predominant. As far as death cells are concerned, FLG was more potent than cocrystals in triggering necrosis and this was significant at doses of 50 and 100 μg mL^{-1} of the compounds (Fig. 12, right-hand graph). This effect was even more marked for apoptosis, while graphene in the form of a glucose cocrys-

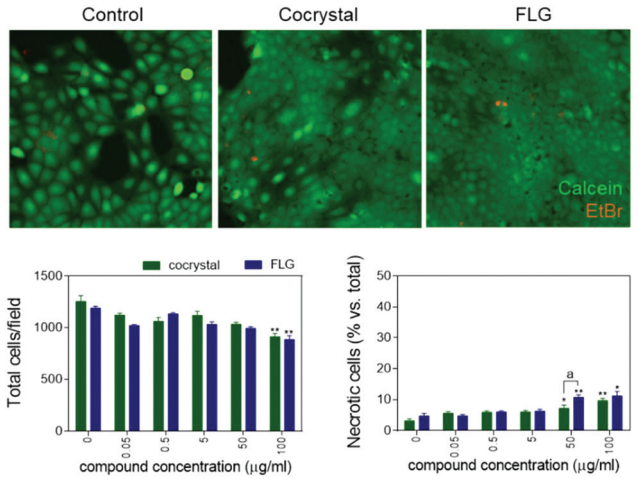

Fig. 12 Effect of cocrystals compared to FLG on HaCaT viability and necrosis.

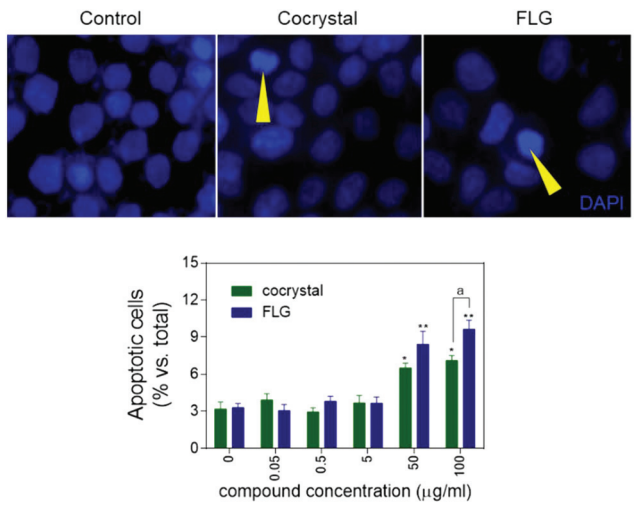

Fig. 13 Effect of cocrystals compared to FLG on HaCaT apoptosis.

tal proved to be less toxic than FLG alone, also at doses of 50 and 100 μg mL^{-1} (Fig. 13).

Pelin *et al.* recently observed significant cellular damage, on the same skin keratinocytes model used in our study, induced by FLG only at high concentrations (>30 μg mL^{-1}) after 72 h from administration.[78] Similar effects were recently reported for other GRMs.[81] The results of this study confirm that combining FLG in cocrystals with glucose is less toxic than FLG alone, which could be related to an increase in solubility, stability in the culture media and probably in cell uptake, as reported recently for GO.[82] Further studies must be performed to ascertain whether the formation of the cocrystal affects the graphene cellular internalization route and if this property can be exploited in active cell targeting. Our efforts will continue in this direction.

Conclusions

A mechanochemical treatment with carbohydrates was successfully applied to exfoliate graphite in a simple and green approach. Of the various carbohydrates tested, glucose showed the best behaviour in terms of exfoliation to generate few layer graphene with a relatively low number of defects, as evidenced by Raman spectroscopy. The addition of molar equivalents of water to the ball milling treatment allowed the formation of glucose-graphene cocrystals. As happens with drugs, glucose-graphene cocrystals form reasonable dispersions in water and have optimal colloidal stability. The glucose-graphene cocrystals were also tested in interactions with skin cells. The results show that the cocrystals were less toxic than pure FLG and this highlights the possibility of using the cocrystals for biological applications of graphene.

Experimental

Computational details

The structural and electronic features of these carbohydrate molecules on graphene were characterised by periodic spin-polarized density functional theory (DFT)[83,84] with standard projector augmented wave (PAW) potentials,[85,86] as implemented in the VASP code.[87–89] The Perdew–Burke–Ernzerhof (PBE)[90,91] functional was used with a kinetic energy cut-off of 750 eV for the plane wave basis set to converge the total energy of our systems within 1 meV fu^{-1}. The supramolecular network was applied using the conjugate gradient method until the forces were below 0.03 eV $Å^{-1}$ on all atoms. Each graphene cell was modelled with a vacuum space larger than 15 Å between repeated images, and dipole corrections were applied.[92]

The dispersion-corrected DFT scheme (DFT-D) proposed by Grimme[93] was employed and in this approach weak interactions are accounted for as a general dispersion correction to the DFT energy given by an attractive semi-empirical pair potential. This methodology is widely reported in the literature for carbon-based nanostructures[94–96] and delivers results that are qualitatively comparable to more expensive computational methods with experimental data. In particular, the most recent DFT-D, *i.e.* DFT-D3, with the Becke–Johnson damping function (BJ)[97,98] as implemented in VASP was applied.

A Γ-centred 21 × 21 × 1 *k*-point Monkhorst–Pack mesh grid was used for the graphene unit cell and appropriate scaling of these values was carried out in each case depending on the size of the supercell under study. The Brillouin zone was integrated with the Gaussian smearing method (0.01 eV as smearing width), except in the case of density of state analysis (PDOS), where the tetrahedron smearing method with Blöchl corrections was used.[99]

Characterization techniques

Powder X-ray diffraction (PXRD). Powder X-ray diffraction (PXRD) data were recorded on a Philips (Panalytical) model

X'Pert MPD diffractometer using Cu KAlpha1 (1.54056 Angstroms) at 40 kV and 40 mA. Diffraction patterns were collected over a range of 5–60° 2θ at a scan rate of 0.01° 2θ min^{-1} and a scan velocity of 0.004° s^{-1}.

Raman spectroscopy. Raman spectra were recorded on an InVia Renishaw microspectrometer equipped with 532 nm point-based laser. In all cases power density was kept below 1 mW μm^{-2} to avoid laser heating effects. Raman samples were measured in solid state under ambient conditions. The resulting spectra (after at least 30–40 random locations on each sample) were fitted with Lorentzian-shaped bands in their D, G and 2D peaks to ascertain band positions, widths and intensities.

UV spectroscopy. UV-Vis spectra were recorded in 1 cm quartz cuvettes on a Cary 5000 UV-vis-NIR spectrophotometer. Dual beam mode and baseline correction were used throughout the measurements to scan the maximum absorbance at 660 nm for FLG, for 2 h and 24 h at different time intervals. The concentration of graphene samples was determined from the optical absorption coefficient at maximum absorbance, using $A = \alpha \cdot l \cdot c$, where l (m) is the light path length, c (g L^{-1}) is the concentration of dispersed graphene material, and α (L g^{-1} m^{-1}) is the absorption coefficient, with α = 690 L g^{-1} m^{-1} at 660 nm FLG. In all cases, the optical absorbance divided by cell length against the concentration exhibited Lambert–Beer behaviour.

Thermogravimetric analysis (TGA). Thermogravimetric analyses (TGA) were performed with a TGA Q50 (TA Instruments) at 10 °C min^{-1} under nitrogen flow, from 100 °C to 800 °C.

Brunauer–Emmett–Teller (BET) experimental setup. The total surface-area concentration and the amount of nitrogen gas required to condensate a monolayer was measured experimentally using BET equipment through isotherms of adsorption and desorption and the distribution of the size of pores. These experiments were measured in a Gemini VII, Micromeritics brand; nitrogen gas was used as an adsorbate and tests were performed at liquid nitrogen temperature (−195.79 °C). For this test, the samples were degassed prior to the adsorption measurements.

Transmission electron microscopy (TEM). TEM analyses were performed on stable dispersions of graphene (the same used for Raman analysis) diluted as necessary and dip-cast on Lacey copper grids (3.00 mm, 200 mesh), coated with carbon film, and dried under vacuum. The sample was investigated using a High-Resolution Transmission Electron Microscope (HRTEM) JEOL 2100 at an accelerating voltage of 100 kV.

Cell culture. HaCaT cells were maintained in high glucose, 4.5 g L^{-1}, DMEM medium (Sigma-Aldrich) containing 10% FBS and 1% antibiotic/antimycotic (Sigma-Aldrich), at 37 °C and 5% CO_2. Experiments were performed in DMEM containing 10% FBS. All cells used in this study were up to the 15th passage.

Determination of apoptosis, necrosis and viability. Cells were seeded in 96 well plates and incubated for 24 h (15.000 cells per well seeded) with increasing concentrations (0.05; 0.5; 5; 50; 100 μg mL^{-1}) of FLG2 and FLG1. After each treatment cells were incubated with 10 μg mL^{-1} EtBr and 1 μM Calcein-AM (Thermo-Fischer). Viable (green) and necrotic cells (red) were determined by Cytation 5 (BioTek) (4 pictures per well). Immediately after image acquisition, cells were fixed, permeabilized for 2 min in ice-cold methanol and stained with 1 μg mL^{-1} Hoescht. Apoptotic nuclei were determined following morphological criteria (nucleus pyknosis, condensation and fragmentation). For viability, results are expressed as total cells and as percentage *vs.* control cells. For necrosis and apoptosis, results are expressed as percentage *vs.* total or control cells in at least 3 independent experiments.

Statistical analysis

Data are expressed as mean ± S.E.M. Statistical analysis was carried out with GraphPad Prism 6, using one-way ANOVA (Kruskal–Wallis test) followed by a statistical test for multiple comparisons (Dunn's test). Differences were considered significant at $*p < 0.05$; $**p < 0.01$; $***p < 0.001$.

Conflicts of interest

There are no conflicts to declare.

Acknowledgements

Financial support from the EU Graphene-based disruptive technologies, Flagship project (no. 696656) and the Spanish Ministerio de Economía y Competitividad (project CTQ2014-53600-R) are gratefully acknowledged. Raman spectra were collected using a Spectrometer confocal Renishaw InVia Reflex (FEDER-JCCM funding, UNCM13-1E-1663), included in the facilities of the Instituto Regional de Investigación Científica Aplicada (IRICA), which is also acknowledged for technical support.

Notes and references

1 L. M. Gilbertson, J. B. Zimmerman, D. L. Plata, J. E. Hutchison and P. T. Anastas, *Chem. Soc. Rev.*, 2015, **44**, 5758–5777.
2 R. S. Varma, *ACS Sustainable Chem. Eng.*, 2016, **4**, 5866–5878.
3 Y. Lu and S. Ozcan, *Nano Today*, 2015, **10**, 417–420.
4 W. Ren and H. M. Cheng, *Nat. Nanotechnol.*, 2014, **9**, 726–730.
5 M. Lotya, P. J. King, U. Khan, S. De and J. N. Coleman, *ACS Nano*, 2010, **4**, 3155–3162.
6 Y. Hong, Z. Wang and X. Jin, *Sci. Rep.*, 2013, **3**, 3439.
7 J. M. Munuera, J. I. Paredes, M. Enterria, A. Pagan, S. Villar-Rodil, M. F. R. Pereira, J. I. Martins, J. L. Figueiredo, J. L. Cenis, A. Martinez-Alonso and J. M. D. Tascon, *ACS Appl. Mater. Interfaces*, 2017, **9**, 24085–24099.
8 M. Yi, Z. Shen, S. Ma and X. Zhang, *J. Nanopart. Res.*, 2012, **14**. Q5

9 S. Zhao, S. Xie, Z. Zhao, J. Zhang, L. Li and Z. Xin, *ACS Sustainable Chem. Eng.*, 2018, **6**, 7652–7661.
10 M. Buzaglo, M. Shtein, S. Kober, R. Lovrincic, A. Vilan and O. Regev, *Phys. Chem. Chem. Phys.*, 2013, **15**, 4428–4435.
11 J. H. Ding, H. R. Zhao and H. B. Yu, *Sci. Rep.*, 2018, **8**, 5567.
12 H. Gao and G. Hu, *RSC Adv.*, 2016, **6**, 10132–10143.
13 H. Tao, Y. Zhang, Y. Gao, Z. Sun, C. Yan and J. Texter, *Phys. Chem. Chem. Phys.*, 2017, **19**, 921–960.
14 H. Gao, K. Zhu, G. Hu and C. Xue, *Chem. Eng. J.*, 2017, **308**, 872–879.
15 X. An, T. Simmons, R. Shah, C. Wolfe, K. M. Lewis, M. Washington, S. K. Nayak, S. Talapatra and S. Kar, *Nano Lett.*, 2010, **10**, 4295–4301.
16 H. Yang, Y. Hernandez, A. Schlierf, A. Felten, A. Eckmann, S. Johal, P. Louette, J. J. Pireaux, X. Feng, K. Mullen, V. Palermo and C. Casiraghi, *Carbon*, 2013, **53**, 357–365.
17 F. Irin, M. J. Hansen, R. Bari, D. Parviz, S. D. Metzler, S. K. Bhattacharia and M. J. Green, *J. Colloid Interface Sci.*, 2015, **446**, 282–289.
18 M. Lotya, Y. Hernandez, P. J. King, R. J. Smith, V. Nicolosi, L. S. Karlsson, F. M. Blighe, S. De, Z. Wang, I. T. McGovern, G. S. Duesberg and J. N. Coleman, *J. Am. Chem. Soc.*, 2009, **131**, 3611–3620.
19 M. C. Duch, G. R. Budinger, Y. T. Liang, S. Soberanes, D. Urich, S. E. Chiarella, L. A. Campochiaro, A. Gonzalez, N. S. Chandel, M. C. Hersam and G. M. Mutlu, *Nano Lett.*, 2011, **11**, 5201–5207.
20 S. Ahadian, M. Estili, V. J. Surya, J. Ramon-Azcon, X. Liang, H. Shiku, M. Ramalingam, T. Matsue, Y. Sakka, H. Bae, K. Nakajima, Y. Kawazoe and A. Khademhosseini, *Nanoscale*, 2015, **7**, 6436–6443.
21 A. Pattammattel and C. V. Kumar, *Adv. Funct. Mater.*, 2015, **25**, 7088–7098.
22 D. W. Johnson, B. P. Dobson and K. S. Coleman, *Curr. Opin. Colloid Interface Sci.*, 2015, **20**, 367–382.
23 D. Bitounis, H. Ali-Boucetta, B. H. Hong, D. H. Min and K. Kostarelos, *Adv. Mater.*, 2013, **25**, 2258–2268.
24 Y. Hernandez, V. Nicolosi, M. Lotya, F. M. Blighe, Z. Sun, S. De, I. T. Mcgovern, B. Holland, M. Byrne, Y. K. G. U. N. Ko, J. J. Boland, P. Niraj, G. Duesberg, S. Krishnamurthy, R. Goodhue, J. Hutchison, V. Scardaci, A. C. Ferrari and J. N. Coleman, *Nat. Nanotechnol.*, 2008, **3**, 563–568.
25 J. N. Coleman, *Acc. Chem. Res.*, 2013, **46**, 14–22.
26 Y. Zhu, S. Murali, W. Cai, X. Li, J. W. Suk, J. R. Potts and R. S. Ruoff, *Adv. Mater.*, 2010, **22**, 3906–3924.
27 D. Chen, H. Feng and J. Li, *Chem. Rev.*, 2012, **112**, 6027–6053.
28 G. Bolla and A. Nangia, *Chem. Commun.*, 2016, **52**, 8342–8360.
29 P. Cerreia Vioglio, M. R. Chierotti and R. Gobetto, *Adv. Drug Delivery Rev.*, 2017, **117**, 86–110.
30 A. Sokal and E. Pindelska, *Curr. Pharm. Des.*, 2018, **24**, 1–9.
31 L. Lange, M. Schleinitz and G. Sadowski, *Cryst. Growth Des.*, 2016, **16**, 4136–4147.
32 S. Karki, T. Friščić, L. Fábián, P. R. Laity, G. M. Day and W. Jones, *Adv. Mater.*, 2009, **21**, 3905–3909.
33 D. Braga, E. Dichiarante, G. Palladino, F. Grepioni, M. R. Chierotti, R. Gobetto and L. Pellegrino, *CrystEngComm*, 2010, **12**, 3534–3536.
34 Y. Gao, H. Zu and J. Zhang, *J. Pharm. Pharmacol.*, 2011, **63**, 483–490.
35 D. Braga, L. Maini and F. Grepioni, *Chem. Soc. Rev.*, 2013, **42**, 7638–7648.
36 T. Friscic, A. V. Trask, W. Jones and W. D. Motherwell, *Angew. Chem., Int. Ed.*, 2006, **45**, 7546–7550.
37 D. Hasa, G. S. Rauber, D. Voinovich and W. Jones, *Angew. Chem., Int. Ed.*, 2015, **54**, 7371–7375.
38 N. Rubio, C. Fabbro, M. A. Herrero, A. de la Hoz, M. Meneghetti, J. L. Fierro, M. Prato and E. Vazquez, *Small*, 2011, **7**, 665–674.
39 R. B. Baig and R. S. Varma, *Chem. Soc. Rev.*, 2012, **41**, 1559–1584.
40 R. S. Varma, *Green Chem.*, 2008, **10**, 1129–1130.
41 M. Yi and Z. Shen, *J. Mater. Chem. A*, 2015, **3**, 11700–11715.
42 I. Y. Jeon, Y. R. Shin, G. J. Sohn, H. J. Choi, S. Y. Bae, J. Mahmood, S. M. Jung, J. M. Seo, M. J. Kim, D. Wook Chang, L. Dai and J. B. Baek, *Proc. Natl. Acad. Sci. U. S. A.*, 2012, **109**, 5588–5593.
43 P. Sun, S. Kuga, M. Wu and Y. Huang, *Cellulose*, 2014, **21**, 2469–2478.
44 S. Balasubramanyan, S. Sasidharan, R. Poovathinthodiyil, R. M. Ramakrishnan and B. N. Narayanan, *New J. Chem.*, 2017, **41**, 11969–11978.
45 V. Leon, J. M. Gonzalez-Dominguez, J. L. Fierro, M. Prato and E. Vazquez, *Nanoscale*, 2016, **8**, 14548–14555.
46 C. A. Beevers, T. R. R. McDonald, J. H. Robertson and F. Stern, *Acta Crystallogr.*, 1952, **5**, 689–690.
47 G. M. Brown and H. A. Levy, *Science*, 1963, **141**, 921–923.
48 A. M. Rodriguez, A. B. Munoz-Garcia, O. Crescenzi, E. Vazquez and M. Pavone, *Phys. Chem. Chem. Phys.*, 2016, **18**, 22203–22209.
49 V. León, A. M. Rodríguez, P. Prieto, M. Prato and E. Vazquez, *ACS Nano*, 2014, **8**, 563–571.
50 V. León, M. Quintana, M. A. Herrero, J. L. G. Fierro, A. de la Hoz, M. Prato and E. Vázquez, *Chem. Commun.*, 2011, **47**, 10936–10938.
51 J. D. Wuest and A. Rochefort, *Chem. Commun.*, 2010, **46**, 2923–2925.
52 J. M. Gonzalez-Dominguez, V. Leon, M. I. Lucio, M. Prato and E. Vazquez, *Nat. Protoc.*, 2018, **13**, 495–506.
53 V. León, G. Castañeda, M. A. Herrero and E. Vázquez, *RSC Adv.*, 2017, **7**, 21982–21987.
54 A. C. Ferrari, *Solid State Commun.*, 2007, **143**, 47–57.
55 A. C. Ferrari and D. M. Basko, *Nat. Nanotechnol.*, 2013, **8**, 235–246.
56 A. A. Green and M. C. Hersam, *Nano Lett.*, 2009, **9**, 4031–4036.
57 A. C. Ferrari, J. C. Meyer, V. Scardaci, C. Casiraghi, M. Lazzeri, F. Mauri, S. Piscanec, D. Jiang, K. S. Novoselov, S. Roth and A. K. Geim, *Phys. Rev. Lett.*, 2006, **97**, 187401.

58 K. R. Paton, E. Varrla, C. Backes, R. J. Smith, U. Khan, A. O'Neill, C. Boland, M. Lotya, O. M. Istrate, P. King, T. Higgins, S. Barwich, P. May, P. Puczkarski, I. Ahmed, M. Moebius, H. Pettersson, E. Long, J. Coelho, S. E. O'Brien, E. K. McGuire, B. M. Sanchez, G. S. Duesberg, N. McEvoy, T. J. Pennycook, C. Downing, A. Crossley, V. Nicolosi and J. N. Coleman, *Nat. Mater.*, 2014, **13**, 624–630.

59 C. Casiraghi, A. Hartschuh, H. Qian, S. Piscanec, C. Georgi, A. Fasoli, K. S. Novoselov, D. M. Basko and A. C. Ferrari, *Nano Lett.*, 2009, **9**, 1433–1441.

60 F. Torrisi, T. Hasan, W. Wu, Z. Sun, A. Lombardo, T. S. Kulmala, G. W. Hsieh, S. Jung, F. Bonaccorso, P. J. Paul, D. Chu and A. C. Ferrari, *ACS Nano*, 2012, **6**, 2992–3006.

61 U. Mogera, R. Dhanya, R. Pujar, C. Narayana and G. U. Kulkarni, *Phys. Chem. Lett.*, 2015, **6**, 4437–4443.

62 A. Mottier, F. Mouchet, C. Laplanche, S. Cadarsi, L. Lagier, J. C. Arnault, H. A. Girard, V. Leon, E. Vazquez, C. Sarrieu, E. Pinelli, L. Gauthier and E. Flahaut, *Nano Lett.*, 2016, **16**, 3514–3518.

63 A. Peigney, C. Laurent, E. Flahaut, R. R. Bacsa and A. Rousset, *Carbon*, 2001, **39**, 507–514.

64 M. J. McAllister, J.-L. Li, D. H. Adamson, H. C. Schniepp, A. A. Abdala, J. Liu, M. Herrera-Alonso, D. L. Milius, R. Car, R. K. Prud'homme and I. A. Aksay, *Chem. Mater.*, 2007, **19**, 4396–4404.

65 J. P. Rourke, P. A. Pandey, J. J. Moore, M. Bates, I. A. Kinloch, R. J. Young and N. R. Wilson, *Angew. Chem., Int. Ed.*, 2011, **50**, 3173–3177.

66 F. Tristan-Lopez, A. Morelos-Gomez, S. M. Vega-Diaz, M. L. Garcia-Betancourt, N. Perea-Lopez, A. L. Elias, H. Muramatsu, R. Cruz-Silva, S. Tsuruoka, Y. A. Kim, T. Hayahsi, K. Kaneko, M. Endo and M. Terrones, *ACS Nano*, 2013, **7**, 10788–10798.

67 M. Shtein, I. Pri-Bar, M. Varenik and O. Regev, *Anal. Chem.*, 2015, **87**, 4076–4080.

68 S. Colonna, O. Monticelli, J. Gomez, C. Novara, G. Saracco and A. Fina, *Polymer*, 2016, **102**, 292–300.

69 N. K. Duggirala, A. Smith, J. Ł. Wojtas, R. D. Shytle and M. J. Zaworotko, *Cryst. Growth Des.*, 2014, **14**, 6135–6142.

70 M. D. Eddleston, B. Patel, G. M. Day and W. Jones, *Cryst. Growth Des.*, 2013, **13**, 4599–4606.

71 M. Matsumoto, Y. Saito, C. Park, T. Fukushima and T. Aida, *Nat. Chem.*, 2015, **7**, 730–736.

72 S. Xiong, S. Chen, S. Jin, Z. Zhang, Y. Zhang and L. Li, *RSC Adv.*, 2017, **7**, 6795–6799.

73 H. D. Clarke, K. K. Arora, H. Bass, P. Kavuru, T. T. Ong, T. Pujari, L. Wojtas and M. J. Zaworotko, *Cryst. Growth Des.*, 2010, **10**, 2152–2167.

74 Z. Ma, H. Zhang, Z. Yang, Y. Zhang, B. Yu and Z. Liu, *J. Mater. Chem. A*, 2014, **2**, 19324–19329.

75 N. K. Duggirala, A. Vyas, J. F. Krzyzaniak, K. K. Arora and R. Suryanarayanan, *Mol. Pharm.*, 2017, **14**, 3879–3887.

76 M. A. Creighton, J. R. Rangel-Mendez, J. Huang, A. B. Kane and R. H. Hurt, *Small*, 2013, **9**, 1921–1927.

77 W. Hu, C. Peng, M. Lv, X. Li, Y. Zhang, N. Chen, C. Fan and Q. Huang, *ACS Nano*, 2011, **5**, 3693–3700.

78 M. Pelin, L. Fusco, V. Leon, C. Martin, A. Criado, S. Sosa, E. Vazquez, A. Tubaro and M. Prato, *Sci. Rep.*, 2017, **7**, 40572.

79 W. Zhang, Y. Sun, Z. Lou, L. Song, Y. Wu, N. Gu and Y. Zhang, *Colloids Surf., B*, 2016, **151**, 215–223.

80 T. Lammel, P. Boisseaux, M. L. Fernandez-Cruz and J. M. Navas, *Part. Fibre Toxicol.*, 2013, **10**, 27.

81 G. Lalwani, M. D'Agati, A. M. Khan and B. Sitharaman, *Adv. Drug Delivery Rev.*, 2016, **105**, 109–144.

82 H. Liu, T. Li, Y. Liu, G. Qin, X. Wang and T. Chen, *Nanoscale Res. Lett.*, 2016, **11**, 211–221.

83 P. Hohenberg and W. Kohn, *Phys. Rev.*, 1964, **136**, B864–B871.

84 W. Kohn and L. J. Sham, *Phys. Rev.*, 1965, **140**, 1133–1138.

85 P. E. Blochl, *Phys. Rev. B: Condens. Matter Mater. Phys.*, 1994, **50**, 17953–17979.

86 G. Kresse and D. Joubert, *Phys. Rev. B: Condens. Matter Mater. Phys.*, 1999, **59**, 1758–1775.

87 G. Kresse and J. Hafner, *Phys. Rev. B: Condens. Matter Mater. Phys.*, 1993, **47**, 558–561.

88 G. Kresse and J. Hafner, *Phys. Rev. B: Condens. Matter Mater. Phys.*, 1994, **49**, 14251–14269.

89 G. Kresse and J. Furthmüller, *Comput. Mater. Sci.*, 1996, **6**, 15–50.

90 J. P. Perdew, K. Burke and M. Ernzerhof, *Phys. Rev. Lett.*, 1996, **77**, 3865–3868.

91 J. P. Perdew, K. Burke and M. Ernzerhof, *Phys. Rev. Lett.*, 1997, **78**, 1396.

92 J. Neugebauer and M. Scheffler, *Phys. Rev. B: Condens. Matter Mater. Phys.*, 1992, **46**, 16067–16080.

93 S. Grimme, *J. Comput. Chem.*, 2006, **27**, 1787–1799.

94 D. Mollenhauer, C. Brieger, E. Voloshina and B. Paulus, *J. Phys. Chem. C*, 2015, **119**, 1898–1904.

95 B. Van Troeye, M. Torrent and X. Gonze, *Phys. Rev. B*, 2016, **93**, 144304.

96 S. Grimme, A. Hansen, J. G. Brandenburg and C. Bannwarth, *Chem. Rev.*, 2016, **116**, 5105–5154.

97 S. Grimme, S. Ehrlich and L. Goerigk, *J. Comput. Chem.*, 2011, **32**, 1456–1465.

98 S. Grimme, J. Antony, S. Ehrlich and H. Krieg, *J. Chem. Phys.*, 2010, **132**, 154104.

99 P. E. Blöchl, O. Jepsen and O. K. Andersen, *Phys. Rev. B: Condens. Matter Mater. Phys.*, 1994, **49**, 16223–16233.